The Journal of the Acoustical Society of America

AUGUST 15 2024

Elasto-plastic friction modeling toward reconstructing measured bowed-string transients

Ewa Matusiak; Vasileios Chatziioannou

J. Acoust. Soc. Am. 156, 1135–1147 (2024)
https://doi.org/10.1121/10.0028228

ASA
ACOUSTICAL SOCIETY OF AMERICA

JASA ARTICLE

Elasto-plastic friction modeling toward reconstructing measured bowed-string transients

Ewa Matusiak[a] and Vasileios Chatziioannou
Department of Music Acoustics—Wiener Klangstil (IWK), University of Music and Performing Arts Vienna, Anton-von-Webern-Platz 1, 1030 Vienna, Austria

ABSTRACT:
Physical modeling may be used to simulate the motion of a vibrating string under frictional excitation by a bow. This study compares the measured transient behavior of a bowed string with predictions from a physics-based simulation that assumes a finite-width bow, incorporates bow-hair compliance, considers the string's torsional motion, and utilizes an elasto-plastic friction model. The model is first evaluated by comparing simulated Guettler playability diagrams to a measured diagram obtained from a robot arm bowing a monochord. The playability regions are qualitatively similar, but some significant differences in the underlying waveforms are not captured. In order to improve the reconstructions of individual waveforms, inverse modeling is employed to derive parameter values for the elasto-plastic friction model, demonstrating the ability to generate accurate reconstructions of measured signal transients. The findings highlight the importance of accounting for variable friction coefficients that change with bow force and bow acceleration. This observation is consistent with prior research indicating that static and dynamic friction coefficients vary within a Guettler diagram.
https://doi.org/10.1121/10.0028228
(Received 16 April 2024; revised 4 July 2024; accepted 29 July 2024; published online 15 August 2024)
[Editor: Andrew Morrison] Pages: 1135–1147

I. INTRODUCTION

Bowed-string instruments have been the subjects of numerous studies in the last few decades, partly because of the complex interaction between the bow and the string. The highly nonlinear dynamics that take place at the bow-string contact point remain a challenging problem for physical modeling attempts. A major unsolved concern in bowed-string modeling is the different behaviors of the system in the sticking phase and in the slipping phase. To this end, several friction models have been developed. One model, hereafter referred to as "classical," was proposed by Smith and Woodhouse,[1] after measurements of the coefficient of friction in a steady-bowing setup. Another model, hereafter referred to as "reconstructed," was obtained from measurements of the coefficients of friction in the transient part of the waveform.[2] Later, Serafin *et al.*[3] used an elasto-plastic friction model, developed in Ref. 4, where the surface of the sliding bow hair against the string is considered as a set of bristles, while Woodhouse[1,5] proposed a thermal friction model where the temperature of rosin is considered. Although qualitative similarities between such models and experimental measurements have been observed, it has been recently shown[6] that the numerical reproduction of a measured time-domain waveform (e.g., string velocity), especially the transient part, has not yet been achieved. For more discussion and recent developments concerning thermal friction models, we refer the reader to Ref. 7.

Rather than looking at individual waveforms, a more qualitative comparison between physics-based simulations and experimental measurements may be achieved by contrasting playability diagrams populated either experimentally or via physical modeling. Schelleng[8] and Guettler[9] suggested two different diagram types to assess the playability of a bowed string, concentrating on different aspects of the string's behavior. Schelleng diagrams focus on the ability of a bowed string to sustain the Helmholtz motion when the bow force and the bow speed are kept constant. A Guettler diagram, on the other hand, deals with the initial transients at the start of a bow stroke when the bow force stays constant and the bow accelerates monotonically from rest (see, e.g., Fig. 1). Attempts to compare physics-based simulations and experimental measurements using Guettler diagrams were carried out in Refs. 2, 6, and 10, where three versions of Guettler diagrams were simulated using three different friction models: "classical,"[1] "reconstructed,"[2] and thermal.[1,5] The obtained results were compared to an experimentally obtained Guettler diagram. The experimental data were collected from two laboratory tests.[11,12] In both experiments, rosin-coated rods were used for the "bow" in order to reduce the bow-string contact area and to be able to use simple simulations of point bowing. Galluzzo and Woodhouse[11] used an acrylic rod of 13 mm diameter coated with rosin and bowed a D-cello string mounted on a cello, while Schumacher and Garoff[12] used a glass rod of 6 mm diameter, dip-coated in rosin to bow a violin E-string mounted on a monochord. It was shown that none of the three models was able to correctly predict the playability region, in terms

[a]Email: matusiak@mdw.ac.at

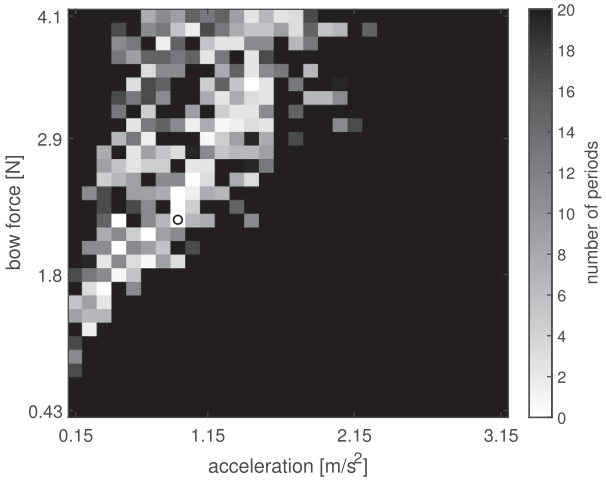

FIG. 1. Experimentally obtained Guettler diagram. Bowing was performed on G-cello string, mounted on a monochord, by a robotic arm holding a real bow positioned at $\beta = 0.0786$. The number of periods of string oscillation that are needed to reach Helmholtz motion is shown on the diagram with different shades of gray. White indicates a perfect transient, black indicates that it took 20 or more period lengths to achieve Helmholtz motion, and shaded gray indicates intermediate cases.

of a Guettler diagram. However, the overall position and shape of the playable wedge-shaped region agreed roughly with the measurements. The "classical" and "reconstructed" friction models predicted a limited playable region, while with the thermal model, it seemed that the string was easier to play (more white pixels in the Guettler diagram). However, as mentioned earlier, the individual waveforms were not correctly reconstructed by either of the models. Recently,[7,13] an enhanced version of the thermal model was presented based on the observations in Ref. 6 and applied to bowing a G-violin string. However, simulated Guettler diagrams using the enhanced thermal model could not be compared to the existing measurements, since due to numerical instabilities, the model could not be used for simulating bowing on longer strings (such as cello strings).

In this work, we set to evaluate the performance of an elasto-plastic model,[4] recently applied to bow-string modeling, from the point of view of playability, in comparison to experimental measurements. The aim is to examine whether it is possible for the elasto-plastic model to accurately reconstruct measured time-domain waveforms. Based on this attempt, insights may be gained in order to inform both this and other friction models.

The elasto-plastic model was previously used for simulating bowed-string instruments.[3,14,15] The model was developed to describe friction between two lubricated metal surfaces; therefore, it has the potential to be a candidate for modeling bow-string friction with rosin being the lubricant. Experimental data are obtained by bowing a monochord using a real bow held by a robotic arm. The bow was placed 5.5 cm away from a termination, which for a string of length $L = 70$ cm corresponds to $\beta = 0.0786$, β being the ratio of the bow position to the length of the string. The Guettler diagram in Fig. 1 is generated by incrementing in small steps the bow acceleration and the bow force under controlled conditions while robot-bowing a G-cello string mounted on a monochord setup (see Refs. 16 and 17 for details regarding the experimental setup). The number of periods of string oscillation that are needed to reach Helmholtz motion is then shown on the diagram with different shades of gray. As predicted from theory,[9] a triangular region of playable notes emerges, where Helmholtz motion is achieved in less than 20 periods of oscillation. Furthermore, the chaotic nature of bowed transients manifests itself in the speckled pattern within this region.

In an attempt to reconstruct these experimental data (transient waveforms and playability diagrams), an elasto-plastic friction model is utilized, in combination with inverse modeling. The physical model parameters are optimized in order to obtain a better match between experimentally measured and numerically obtained time-domain waveforms for a single transient signal, marked with a circle in Fig. 1. Two slightly different forms of a friction curve are chosen to simulate the bow-string interaction. After showing a comparison between measured and synthesized transient signals, Guettler diagrams are numerically generated, by using the optimized parameters, and compared to an experimentally obtained one.

Section II presents the model that is used for the simulations, followed by numerical discretization details in Sec. III. Section IV shows the reconstruction of the transient waveform mentioned above via optimization, while Sec. V presents Guettler diagrams obtained numerically and postulates the need to vary the underlying friction model parameters for different bow force and acceleration values. The findings of the study are summarized and discussed in Sec. VI.

II. BOW-STRING INTERACTION MODEL

In the present model, we consider transverse motion as well as torsional motion of the string and couple them to the equation describing the bow-hair compliance. The equation describing transverse waves of the string u can be written as[18–20]

$$\rho A \partial_t^2 u = T \partial_x^2 u - EI \partial_x^4 u,$$

where ρ is the material density, $A = \pi r^2$ is the cross-sectional area of the string with radius r, T is the tension of the string, E is the Young's modulus, and $I = \pi r^4/4$ is the area moment of inertia. The subscripts t and x denote differentiation with respect to time and space, respectively. Damping is an important aspect of the string motion. When using finite-difference methods for solving partial differential equations, as we will do in Sec. III, employing a simple model by Bensa *et al.*[21] is suitable to guarantee passivity. In that scenario, frequency independent σ_0 and frequency dependent σ_1 damping coefficients are incorporated into the equation governing the transverse motion of the string,

$$\rho A \partial_t^2 u = T \partial_x^2 u - EI \partial_x^4 u - 2\sigma_0 \rho A \partial_t u + 2\sigma_1 \rho A \partial_t \partial_x^2 u - f, \quad (1)$$

where f is a distributed friction force. A more detailed version of damping, suitable for space-time solutions and

https://doi.org/10.1121/10.0028228

closest to the damping model obtained in Ref. 22, was suggested by Desvages *et al.* in Ref. 23. That characterization is computationally expensive and requires accurate experimental string characterisation. In this work, we decided to use inverse modeling, based on measured time-domain signals, to obtain the desired damping coefficients and opted for a simpler characterization in order to reduce the number of parameters to be optimized.

In order to include torsional motion of the string in the model, the equation describing transverse motion of the string is coupled, through the distributed friction force f, to the equation describing the torsional movement of the string ω,

$$\theta\,\partial_t^2\omega = K_T\,\partial_x^2\omega - 2\sigma_2\theta\,\partial_t\omega + rf, \tag{2}$$

where θ denotes the polar moment of inertia, K_T indicates torsional stiffness, and σ_2 is a torsional damping coefficient.

Following Ref. 24, the bow is modeled as a simple "spring-dashpot." The bow stick is regarded as a rigid frame moving at a given velocity, v_B, and supporting a ribbon of compliant bow hair. The equation describing the displacement of the bow hair, η, is given by

$$f = -K\eta - D\partial_t\eta, \tag{3}$$

where the distributed spring and damping constants are denoted K and D, respectively.

The relative bow-string velocity can then be expressed as

$$v = (\partial_t u - r\partial_t\omega) - (v_B - \partial_t\eta), \tag{4}$$

where v_B is the bow velocity. The quantities, u, η, v, and f are functions of time $t>0$ and space coordinate $x\in[0,L]$ for the string of length L. For the transverse movement of the string, we assume simply supported ends, meaning that the boundary conditions are

$$u(x,t)|_{x=0,L} = 0\,, \quad \partial_x^2 u|_{x=0,L} = 0, \tag{5}$$

and for the torsional movement, we assume fixed boundary conditions, that is

$$\omega(x,t)|_{x=0,L} = 0. \tag{6}$$

To solve the system, a fourth equation—one describing the friction force f—is needed. There are many models for the friction force to choose from, and many were already investigated from the point of view of Guettler diagrams.[2,6,10] In this work, we have opted for the elasto-plastic friction model,[4] which is a dynamic friction model that establishes a relationship between relative velocity and friction force through a differential equation. It has been already used in simulating the interaction between a bow and string in Refs. 3, 14, 15, and 25. Unlike other friction models found in the literature, the elasto-plastic model considers pre-sliding behavior for minute displacements, where friction gradually increases with displacement. It effectively captures frictional phenomena at low velocities, such as stick-slip motion, pre-sliding behavior, and frictional memory.

The elasto-plastic friction model assumes that the two surfaces, the bow and the string, are irregular at the microscopic level, and their contact is modeled through an ensemble of elastic bristles, each contributing to the total friction load. The idea is that the bow and the string in the contact area are connected with bristles, and as the bow drives the string, the bristles stretch to the point of breaking and the string starts to slide. The bristles are modeled as damped stiff springs, and when the strain exceeds a certain breakaway threshold, the bristles break, and the two surfaces begin to slide. Denoting by z the average bristle deflection and by v the relative velocity between the string and the bow, the friction force is given by[4]

$$f(v,z) = s_0 z + s_1\partial_t z, \tag{7}$$

where $\partial_t z$ is the time derivative of z and is related to v through

$$\partial_t z = v\left(1 - \alpha(v,z)\frac{z}{z_{\rm ss}(v)}\right). \tag{8}$$

s_0 denotes the stiffness and s_1 the damping of the bristles. The relation between z and v, Eq. (8), is defined through $z_{\rm ss}$, the steady-state displacement of the bristles for constant sliding velocities, and $\alpha(v,z)$, the adhesion map between the bow and the string. The latter describes the three states of deformation: elastic, plastic, and the transition between the two. It is defined, for $\mathrm{sign}(v) = \mathrm{sign}(z)$, as

$$\alpha(v,z) = \begin{cases} 0\,, & |z| \le z_{\rm ba}, \\ \alpha_m(v,z)\,, & z_{\rm ba} < |z| < |z_{\rm ss}(v)|, \\ 1\,, & |z| \ge |z_{\rm ss}(v)|, \end{cases} \tag{9}$$

and $\alpha(v,z) = 0$, for $\mathrm{sign}(v) \neq \mathrm{sign}(z)$, where $z_{\rm ba}$ is the breakaway displacement—that is, the moment when the bristles start to break. The breakaway displacement is bounded from above by $\mu_C f_N/s_0$, where μ_C is a dynamic friction coefficient and f_N denotes the normal force applied by the bow. Throughout the paper, we set $z_{\rm ba} = 0.7\mu_C f_N/s_0$.

One way to model the adhesion map is to define α_m as[4]

$$\alpha_m(v,z) = \frac{1}{2}(1 + \mathrm{sign}(z)\sin(\pi\,\theta(v,z))), \tag{10}$$

where

$$\theta(v,z) = \frac{z - \mathrm{sign}(z)\frac{1}{2}(|z_{\rm ss}(v)| + z_{\rm ba})}{|z_{\rm ss}(v)| - z_{\rm ba}}. \tag{11}$$

For small displacements of the bristles, characterized by $|z| \le z_{\rm ba}$, the parameter $\alpha(v,z)$ equals zero, resulting in $\partial_t z = v$ (indicating elastic pre-sliding). However, as

displacements increase beyond z_{ba} but remain below $|z_{ss}(v)|$, certain bristles begin to fracture, initiating a mixed elasto-plastic sliding regime. Upon reaching $|z| \geq |z_{ss}(v)|$, all bristles break, leading to a purely plastic state where the string slips under the bow. Here, $\alpha(v,z) = 1$ and the bristle displacement remains constant over time ($\partial_t z = 0$), establishing a steady-state condition where $z = z_{ss}(v)$ (refer to Fig. 3 in Ref. 25 for more details).

For the steady-state displacement for constant velocities, it is customary to use a Stribeck friction curve,[26]

$$z^1_{ss}(v) = \frac{f_N}{s_0}\text{sign}(v)(\mu_C + (\mu_S - \mu_C)e^{-(v/v_S)^2}), \tag{12}$$

where v_S denotes Stribeck velocity and μ_S is a static friction coefficient. We will refer to this version of the model as the S-model and to z^1_{ss} as an S-curve. Additionally, we will consider another curve for the steady state,

$$z^2_{ss}(v) = \frac{f_N}{s_0}\text{sign}(v)(\mu_C + (\mu_S - \mu_C)e^{-|v|/\epsilon}), \tag{13}$$

where ϵ is between 0.1 and 1. We refer to this version of the model as the ϵ-model and to z^2_{ss} as an ϵ-curve. Galluzzo in Ref. 2 was the first to suggest such a curve, with $\epsilon = 0.7$ in the context of static-friction modeling. It was obtained by fitting a curve to the observed values of limiting static and dynamic friction coefficients during transients. This approach is extended here to an elasto-plastic version, as shown in Eq. (13).

The parameters v_S in z^1_{ss} and ϵ in z^2_{ss} specify the steepness of the curve, and in that respect, the transition from sticking to slipping (see Fig. 2). The smaller v_S, respectively ϵ, the shorter the mixed elasto-plastic state.

The elasto-plastic model with steady-state function z^1_{ss} has been already implemented based on a finite-difference method in Ref. 14, where it was applied to point-bowing a stiff string. The focus of that article was on real-time implementations and not on reproducing measured signals. A comparison of the elasto-plastic model and a thermal model, introduced in Ref. 1, was presented in Ref. 3 using a digital waveguide implementation. That analysis concentrated on bringing out differences and similarities between those two dynamic friction models. The numerical stability of a finite-difference implementation of the elasto-plastic model is analyzed in Ref. 27. We suggest a different discretization approach to ensure that the discrete system energy remains positive for numerical stability reasons.

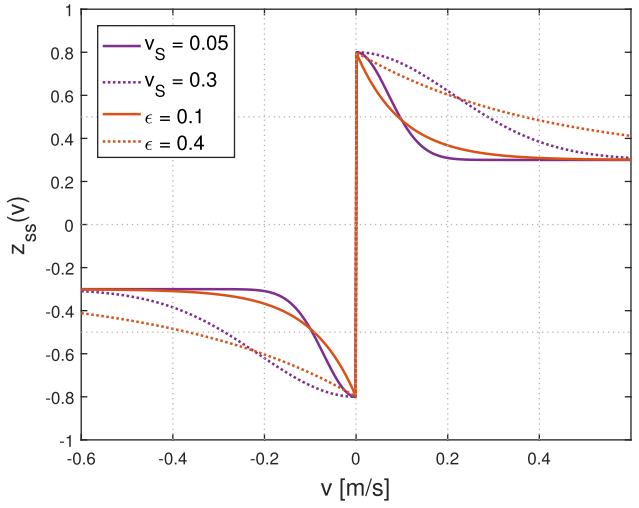

FIG. 2. (Color online) Two choices for the steady-state displacement function, z^1_{ss} in purple and z^2_{ss} in orange, as a function of the relative velocity between the string and the bow. The dotted plots in corresponding colors are for different values of v_S and ϵ, respectively.

III. DISCRETIZATION

A common approach for numerically simulating a bowed string involves employing finite-difference time-domain methods. Various authors have described finite-difference schemes for both the isolated string and the bowed string (see, for instance, Refs. 20 and 24). To establish notation, consider x^L_B and x^R_B as the positions along the string corresponding to the inner and outer edges of the bow width, respectively, with the bow's center situated at x_B. Let M denote the desired number of discrete string locations beneath the bow, denoted by x_m. In the case where $M = 1$, the model assumes point bowing, with $x_M = x_B$.

The model is discretized both temporally and spatially using functions u^n_l that approximate $u(x,\ t)$ at positions $(l\Delta_x, n\Delta_t)$. Temporal discretization is performed with $t = n\Delta_t$, where $\Delta_t = 1/f_s$ and f_s represents the sampling rate, with $n \in \mathbb{N}$. Spatial discretization is achieved with $x = l\Delta_x$, where the grid spacing Δ_x for the string's transverse motion must satisfy the following stability criterion,[20]

$$\Delta_x \geq \sqrt{\frac{\gamma + \sqrt{\gamma^2 + 16\kappa^2\Delta_t^2}}{2}}, \tag{14}$$

where $\gamma = c^2\Delta_t^2 + 4\sigma_1\Delta_t$, with $c = \sqrt{T/\rho A}$ representing the wave speed and $\kappa = \sqrt{EI/\rho A}$ being a stiffness coefficient. The grid points are indexed by $l \in 0, \ldots, N$, where $N = \lfloor L/\Delta_x \rfloor$, resulting in a total of $N+1$ grid points. For the torsional motion of the string, temporal discretization mirrors that of the transverse motion, while spatial discretization is governed by $x = l\Delta^T_x$, where the grid spacing Δ^T_x has to satisfy[20]

$$\Delta^T_x \geq c_T\Delta_t, \tag{15}$$

with $c_T = \sqrt{K_T/\theta}$ representing the torsional wave speed. The grid points are indexed by $l \in 0, \ldots, N_T$, where $N_T = \lfloor L/\Delta^T_x \rfloor$, yielding a total of $N_T + 1$ grid points. Given that torsional waves propagate much faster than transverse waves, the number of grid points N_T is considerably smaller than N.

For a point, x_m, beneath the bow, interpolation operators $I(x_m)$ and $I_T(x_m)$ are utilized to interpolate the string displacement at that position for transverse and torsional motion, respectively. $I(x_m)$ is a row vector of size $N+1$

https://doi.org/10.1121/10.0028228

acting on the column vector $u^n = [u_0^n, \ldots, u_N^n]^T$, while $I_T(x_m)$ is a row vector of size $N_T + 1$ acting on the column vector $\omega^n = [\omega_0^n, \ldots, \omega_{N_T}^n]^T$. Conversely, a spreading operator, $J(x_m)$, represents a column vector responsible for distributing the friction force around the bowing point x_m on the grid $l\Delta_x$. Similarly, $J_T(x_m)$ is a spreading operator that distributes the friction force around the bowing point x_m on the grid $l\Delta_x^T$. The spreading and interpolation operators are related to each other through

$$J(x_m) = \frac{1}{\Delta_x} I(x_m)^T, \quad J_T(x_m) = \frac{1}{\Delta_x^T} I_T(x_m)^T.$$

The approximations of continuous derivatives present in Eqs. (1)–(3) are the operators

$$\begin{aligned}
\delta_{t+} &= \frac{1}{\Delta_t}\left(e_t^+ - 1\right), \quad \delta_{t-} = \frac{1}{\Delta_t}(1 - e_t^-),\\
\delta_{t\cdot} &= \frac{1}{2\Delta_t}\left(e_t^+ - e_t^-\right), \quad \delta_{tt} = \frac{2}{\Delta_t}(\delta_{t\cdot} - \delta_{t-}),\\
\delta_{xx} &= \frac{2}{\Delta_x}(\delta_{x\cdot} - \delta_{x-}), \quad \delta_{xxxx} = \delta_{xx}\,\delta_{xx}\,,
\end{aligned} \tag{16}$$

where $e_t^+ u_l^n = u_l^{n+1}$, $e_t^- u_l^n = u_l^{n-1}$, $e_x^+ u_l^n = u_{l+1}^n$, $e_x^- u_l^n = u_{l-1}^n$, and $1u_l^n = u_l^n$. We will also use central averaging operators

$$\mu_{t-} = \frac{1 + e_t^-}{2}$$

and

$$\mu_{t\cdot} = \frac{e_t^+ + e_t^-}{2}.$$

To simplify the notation, we first divide Eq. (1) by ρA and then discretize it to obtain

$$\begin{aligned}
\delta_{tt} u^n = {} & c^2 \delta_{xx} u^n - \kappa^2 \delta_{xxxx} u^n - 2\sigma_0 \delta_{t\cdot} u^n \\
& + 2\sigma_1 \delta_{t-} \delta_{xx} u^n - (M\rho A)^{-1} \mathcal{J} f(v^n, z^n),
\end{aligned} \tag{17}$$

where $\mathcal{J} = [J(x_1)|\ldots|J(x_M)]$ and $f(v^n, z^n)$ is a column vector with M rows, where each row describes the friction for a point, x_m, of the string that is in contact with the bow,

$$f(v_m^n, z_m^n) = s_0 \mu_{t-} z_m^n + s_1 g(v_m^n, z_m^n) \tag{18}$$

and

$$g(v_m^n, z_m^n) = v_m^n \left[1 - \alpha(v_m^n, \mu_{t-} z_m^n) \frac{\mu_{t-} z_m^n}{z_{\mathrm{ss}}(v_m^n)}\right]. \tag{19}$$

Assuming simply supported ends, the boundary conditions imply

$$u_0^n = u_N^n = 0\,, \quad u_{-1}^n = -u_1^n\,, \quad u_{N+1}^n = -u_{N-1}^n \tag{20}$$

for all $n \in \mathbb{N}$.

Similarly, we divide Eq. (2) by θ and discretize it as

$$\delta_{tt} \omega^n = c_T^2 \delta_{xx} \omega^n - 2\sigma_2 \delta_{t\cdot} \omega^n + \frac{r}{M\theta} \mathcal{J}_T f(v^n, z^n), \tag{21}$$

where $\mathcal{J}_T = [J_T(x_1)|\cdots|J_T(x_M)]$. Assuming fixed ends, the boundary conditions imply

$$\omega_0^n = 0\,, \quad \omega_{N_T}^n = 0 \tag{22}$$

for all $n \in \mathbb{N}$.

Finally, we divide Eq. (3) by D and discretize it as

$$\delta_{t\cdot} \eta_m^n = -\frac{K}{D} \mu_{t\cdot} \eta_m^n - \frac{f(v_m^n, z_m^n)}{MD}. \tag{23}$$

Here, for each point x_m under the bow, the bow-hair compliance is computed. Then, if the bow velocity at time $n\Delta_t$ is v_B^n, the relative velocities at the points of the string in contact with the bow can be discretized as

$$v^n = (\mathcal{I}\delta_{t\cdot} u^n - r\mathcal{I}_T \delta_{t\cdot} \omega^n) - (v_B^n - \delta_{t\cdot} \eta^n), \tag{24}$$

where $\mathcal{I} = [I(x_1)|\ldots|I(x_m)]^T$, $\mathcal{I}_T = [I_T(x_1)|\cdots|I_T(x_m)]^T$, and $\delta_{t\cdot}\eta^n$ is a column vector with m-th entry given by Eq. (23). Let $\mathcal{E}$ be an $M \times M$ identity matrix and

$$\mathcal{L} = \frac{1}{\sigma M \rho A} \mathcal{I}\mathcal{J} + \frac{r^2}{\sigma_T M \theta} \mathcal{I}_T \mathcal{J}_T + \frac{1}{M(D + K\Delta_t)} \mathcal{E}.$$

Utilizing the expression in Eq. (16) for the discrete operator δ_{tt}, as suggested in Ref. 20, and using Eq. (23), we obtain

$$\mathcal{L} \cdot f(v^n, z^n) + v^n - s^n + v_B^n = 0, \tag{25}$$

where $f(v^n, z^n)$ is an M-column vector with entries $f(v_m^n, z_m^n)$ given in Eq. (18) and s^n is an M-column vector with entries given by $s_m^n = \sigma^{-1} a_m^n - \sigma_T^{-1} b_m^n + c_m^n$. Here, $\sigma = (2/\Delta_t) + 2\sigma_0$, $\sigma_T = (2/\Delta_t) + 2\sigma_2$ and

$$\begin{aligned}
a_m^n &= I(x_m)\left[c^2 \delta_{xx} u^n - \kappa^2 \delta_{xxxx} u^n + 2\sigma_1 \delta_{t-} \delta_{xx} u^n + \frac{2}{\Delta_t} \delta_{t-} u^n\right],\\
b_m^n &= I_T(x_m)\left[r c_T^2 \delta_{xx} \omega^n + \frac{2r}{\Delta_t} \delta_{t-} \omega^n\right],\\
c_m^n &= -\frac{K}{D + K\Delta_t} e_t^- \eta_m^n.
\end{aligned}$$

The relation in Eq. (25) gives M equations with $2M$ unknowns. The other M equations are obtained through

$$g(v^n, z^n) - p^n = 0, \tag{26}$$

where the entries of $g(v^n, z^n)$ are given by Eq. (19) and p^n is an M-column vector with entries $p_m^n = \delta_{t-} z_m^n$ and $m = 1, \ldots, M$. Equations (25) and (26) are then solved for v_m^n and z_m^n using the multivariate Newton's method.

The energy conservation property for that friction model in the continuous case was shown by Olsson.[28] It can be shown that the discretization presented above results in an energy-preserving scheme. Proving this is outside the scope of this paper.

IV. CASE STUDY: WAVEFORM RECONSTRUCTION

The performance of the model is first tested on a specific case study. A waveform is reconstructed that was obtained by bowing a G-cello string mounted on a monochord at the relative bow position $\beta = 0.0786$ (that is 0.055 m into the string of length $L = 0.7$ m), with bow acceleration $a = 0.8722$ m/s^2 and bow force $f_N = 2.3433$ N/m, using the robotic arm. The physical parameters of the string, listed in the top part of Table I, were obtained from measurements. The parameters concerning frequency dependent and independent damping were optimized using the Rosenbrock[29] optimization method in order to match a measured steady-state velocity signal, considering only the transverse motion of the string and a static friction model.[20]

The objective function for the optimization is

$$E_{\text{obj}}(F) = \zeta||F_b^m - F_b||_2 + (1-\zeta)||\widehat{F_b^m} - \widehat{F_b}||_2,$$

where F_b^m is the measured bridge force and $\widehat{F_b^m}$ its Fourier transform. F_b is the simulated bridge force, with $\widehat{F_b}$ its Fourier transform. A weight factor, ζ, takes values between 0 and 1 shifting the focus of the objective function towards time-domain ($\zeta \to 1$) or frequency-domain ($\zeta \to 0$) properties. The goal is then to find parameters of the model for which the simulated bridge force F minimizes E_{obj}.

After determining string damping parameters, the optimization for the parameters of the elasto-plastic friction model and those related to torsional movement of the string and bow-hair compliance were performed in steps. We used the same objective function and the Rosenbrock optimization method. Starting with the S-model, we first set $\zeta = 0$ and search for the friction parameters, assuming solely transverse string motion (without torsional waves and bow-hair compliance). These are stiffness and damping coefficients of the bristles, s_0 and s_1, respectively, dynamic μ_C and static μ_S friction coefficients, as well as the Stribeck velocity vS. In that first step, the optimization was performed on the steady-state part of the measured signal. The newly obtained parameters were used as a starting point for another optimization step, now using the transient part of the signal (the first 0.12 s) to further refine the obtained parameters described above. These were finally used as the starting point in minimizing E_{obj} for the whole set of parameters, including torsional waves, bow-hair physics, and frictional forces. This final step aimed to reconstruct the full measured waveform (transient plus steady state) of 0.39 s duration. The obtained values are listed in Table I, marked by an * (with parameters optimized starting from the parameters in the literature, as shown in Table II), and in Table III (S-model).

In order to find the friction parameters in the ϵ-model, we kept fixed the parameters concerning the physics of the string and the bow, listed in Table I, as a "ground truth," and only the parameters related to the ϵ-curve in the elasto-plastic model were optimized. The optimization was performed on the whole measured signal using the objective function E_{obj} with $\zeta = 0$ and the Rosenbrock optimization method. The obtained values are listed in Table III (ϵ-model).

The simulated bridge forces using the parameters obtained from the optimization method are plotted in comparison to the measured waveform in Fig. 3 using the S-model and in Fig. 4 using the ϵ-model. Throughout the article, the purple color in the plots will always refer to a

TABLE I. Physical parameters of the cello G-string and the bow used in the setup.

Parameter[a]	Value
Length (L)	0.7 m
Material density (ρ)	10 059 kg/m^3
Radius (r)	5×10^{-4} m
Tension (T)	149.6 N
Young's modulus (E)	1.37×10^{10} Pa
Wave speed (c)	137.2 m/s
Fundamental frequency (f_0)	98 Hz
Frequency independent damping* (σ_0)	1.537 14 s^{-1}
Frequency dependent damping* (σ_1)	0.0087 m^2/s
Torsional wave speed* (c_T)	849.53 m/s
Polar moment of inertia* (θ)	4.2×10^{-10} kg · m
Torsional stiffness* (K_T)	3.0312×10^{-4} N · m^2
Torsional Q factor* (Q)	29
Bow-hair width	0.01 m
Bow-hair spring constant* (K)	4.8297×10^6 N/m^2
Bow-hair damping constant* (D)	5.7674×10^3 kg/(s · m)

[a]Parameters denoted with an * were optimized starting from the parameters given in the literature (see Table II).

TABLE II. Initial values, taken from the literature, of the parameters used in the inverse modeling procedure.

Parameter	Value
Frequency independent damping (σ_0)	1 s^{-1}
Frequency dependent damping (σ_1)	0.005 m^2/s
Torsional wave speed (c_T)	810 m/s
Polar moment of inertia (θ)	4.2×10^{-10} kg m
Torsional stiffness (K_T)	2.755×10^{-4} N m^2
Torsional Q factor (Q)	34
Bow-hair spring constant (K)	6×10^6 N/m^2
Bow-hair damping constant (D)	3×10^3 kg/(s·m)

TABLE III. Estimated parameters obtained using inverse modeling to approximate the measured bridge force signal for different versions of the elasto-plastic model.

	Result for:		
Parameter	Initial model	S-model	ϵ-model
s_0 (N/m)	10.8×10^4	3.1860×10^5	2.4099×10^5
s_1 (kg/s)	0.000 81	0.0027	0.0115
v_S (m/s)	0.18	0.2280	
ϵ	0.7		0.4
μ_C	0.35	0.5071	0.3382
μ_S	1	1.0207	1.1489

https://doi.org/10.1121/10.0028228

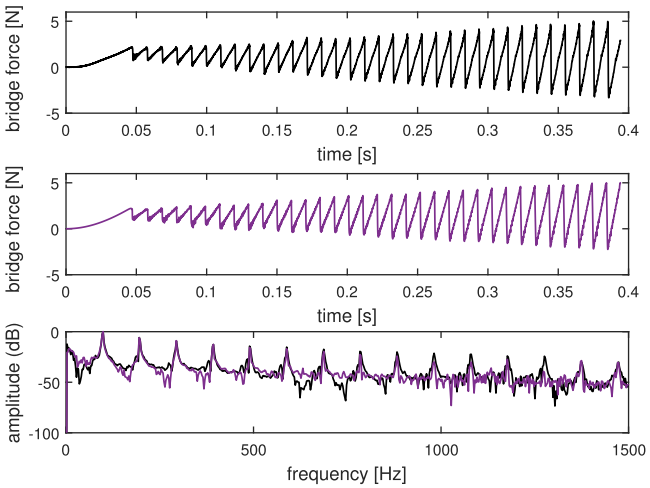

FIG. 3. (Color online) In black (the top plot) is the measured signal obtained by bowing a G-cello string at position given by $\beta = 0.0786$ with bow acceleration $a = 0.8722$ m/s^2 and bow force $f_N = 2.3433$ N/m. Below, in purple, is a simulated reconstructed signal with parameters listed in Tables I and III for the S-curve. The bottom plot shows the respective frequency spectra.

simulation using the elasto-plastic S-model and the orange color will refer to a simulation using the ϵ-model. The general shape of the reconstructed signals agrees with the experimentally measured waveform, while the magnitude of the first slip is also well captured.

As was mentioned before, the elasto-plastic model exhibits a hysteresis loop. The friction force as a function of relative velocity for the two versions of the elasto-plastic model is plotted in Fig. 5. As expected, the shapes of the loops are slightly different, each following the underlying steady-state friction characteristic (z^1_{ss} in the purple plot and z^2_{ss} in the orange plot). The hysteresis loops qualitatively agree with the ones observed on measured signals in Refs. 1, 30, and 31.

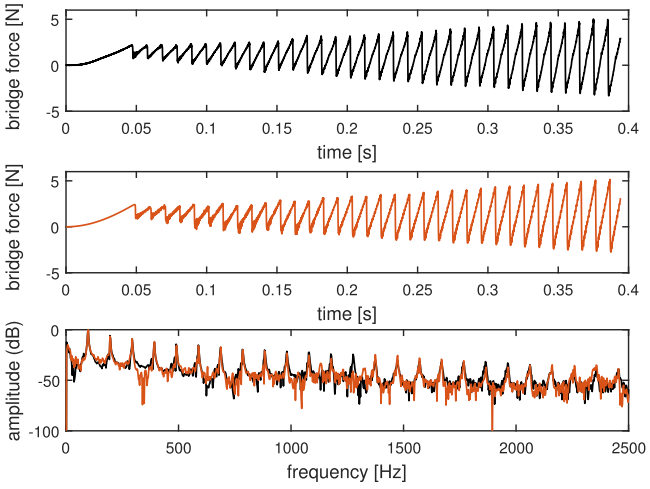

FIG. 4. (Color online) In black (the top plot) is the measured signal obtained by bowing a G-cello string at position given by $\beta = 0.0786$ with bow acceleration $a = 0.8722$ m/s^2 and bow force $f_N = 2.3433$ N/m. Below, in orange, is a simulated signal with parameters listed in Tables I and III for the ϵ-model. The bottom plot shows the respective frequency spectra.

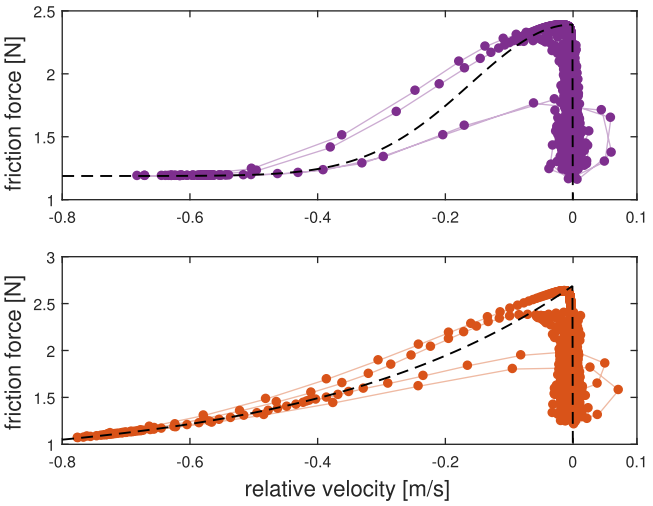

FIG. 5. (Color online) Hysteresis loops for the S-model (top) and ϵ-model (bottom) versions of the friction model. Dashed black lines correspond to the steady-state displacement functions z^1_{ss} and z^2_{ss}.

Despite the successful resynthesis of the measured transient signal, one should still consider the chaotic behavior of the system, as evident by all available measured Guettler diagrams. Small changes in any model parameter may have drastic effects on the ability of the system to reach Helmholtz motion. From an optimization point of view, this results in several local minima being present in the parameter search space. In Sec. V, after presenting Guettler diagrams generated with the above models, we also explore the possibility of a post-processing optimization step, in order to better resynthesize signals that were initially very different from the measured target signals.

V. GUETTLER DIAGRAMS

In order to verify the performance of the elasto-plastic model, two Guettler diagrams were simulated, each corresponding to the two different cases of the elasto-plastic model, as described in Sec. II. In the simulations, the parameters listed in Tables I and III were used and kept constant for different combinations of bow acceleration and bow force.

An experimentally obtained Guettler diagram is shown in Fig. 6 (top). Again, the data were captured by robot-bowing a monochord (G-cello string) at 5.5 cm away from a rigid termination, which corresponds to $\beta = 0.0786$. The measurements were made on a grid of 30×30 data points, linearly spaced in the force $-$ acceleration plane. The chosen range of bow force was from 0.43 N to 4.1 N, and the chosen range of bow acceleration was from 0.15 m/s^2 to 3.15 m/s^2. The time taken to achieve Helmholtz motion relative to the time of the first slip at the given combination of bow force and acceleration is indicated by the shade of the pixel at the corresponding location in the Guettler diagram. White pixels indicate perfect transients (1 period), black pixels indicate that no Helmholtz motion was achieved after 20 periods, and the shaded gray pixels indicate intermediate

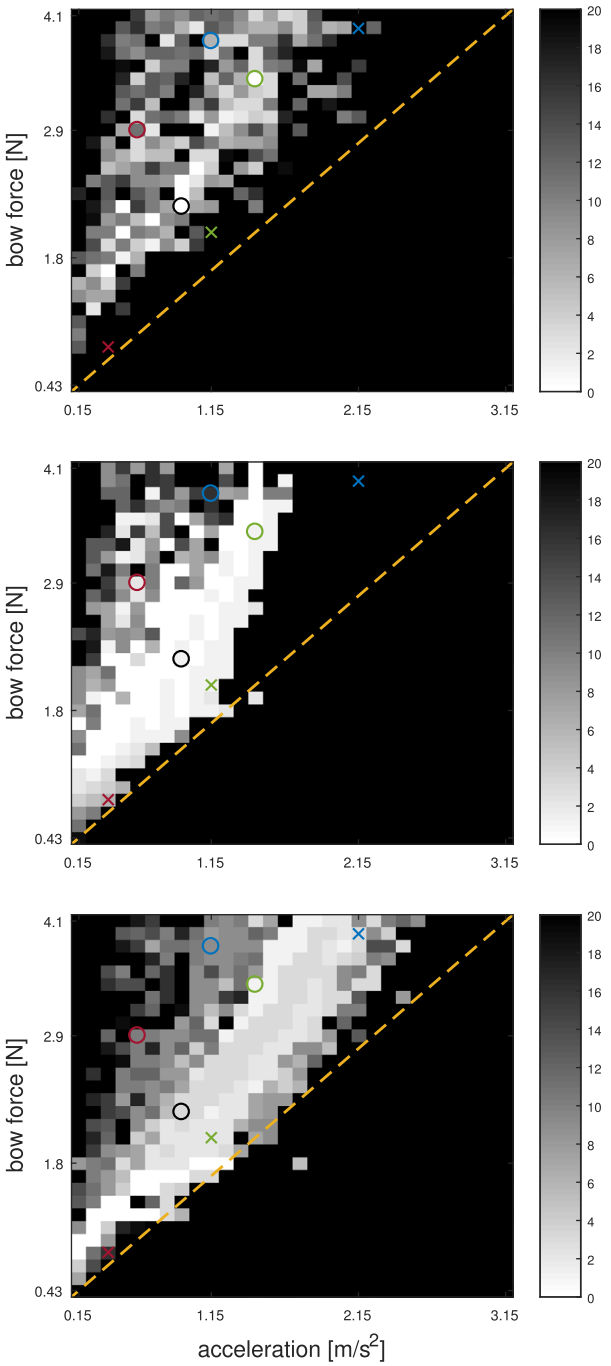

FIG. 6. (Color online) Guettler diagrams from top to bottom: measured, simulated with an S-curve using parameters from the Table III S-model, and simulated using an ϵ-curve with parameters from the Table III ϵ-model.

cases. The choice of 20 periods as a limit was chosen to be consistent with existing comparisons of experimental Guettler diagrams in the literature,[6] and it does not imply that a 20-period transient is necessarily short enough to be musically acceptable. The algorithm used to determine the length of the transient was implemented according to Ref. 2.

When it comes to comparisons with simulated results, two aspects can be considered: (i) a global one, where the attention should be focused on qualitative aspects, that is, the position and shape of the general region within which non-black pixels occur, and the nature of these playable regions; and (ii) a local one, where the reconstruction of individual waveforms is evaluated.

The middle and bottom Guettler diagrams in Fig. 6 were generated by simulations using the two versions of the elasto-plastic friction model. For the middle diagram, we used the S-curve and the parameters from Tables I and III (S-model). For the bottom Guettler diagram, we used the ϵ-curve and the parameters from Tables I and III (ϵ-model). The model parameters have been optimized, as mentioned in Sec. IV, in order to match the waveform that corresponds to the black circle in the Guettler diagrams. The results are directly comparable to the experimental results. The same values of bow position, bow force, and acceleration were used, and the length of the pre-Helmholtz transient was determined using the same algorithm.

The general shape of the playability region and the patchiness of both simulated diagrams agree roughly with the diagram obtained from the measurements. However, both simulated diagrams show a larger "playable" area than the measurements suggest. For easier visual comparison, in each Guettler diagram we plotted a diagonal, yellow dashed line. The model using the ϵ-curve shows yet a larger playable area than the one using the S-curve, with the region of playability spreading further down along the diagonal.

Radial regions containing apparently similar transients are clearly visible in both simulated Guettler diagrams, towards the diagonal. Such radial behaviour was also observed before in simulated diagrams.[2] In the experimental Guettler diagram, such a pattern is not immediately visible. However, by close inspection of individual waveforms, a similar tendency emerges. That is, on the radial regions where the ratio of bow force to bow acceleration is roughly constant, similar waveforms, different only in amplitude, appear. A similar observation was reported in Ref. 2.

Looking at the individual waveforms, we observed that transient signals within the playable region are, in general, well reconstructed. Examples of such waveforms are marked on the Guettler diagrams by colored (red, green, and blue) circles, and their simulated counterparts are shown in Fig. 7. The color of the measured signal corresponds to the position in the Guettler diagram: in purple is the simulated signal using the S-model, while in orange is the simulated signal using the ϵ-model. In all three examples, the transient as well as the steady state for different bow force and acceleration pairs are predicted by both models.

However, not all waveforms are well reconstructed. Marked in red, green, or blue are three such waveform examples corresponding to the red, green, or blue $\times$ in the Guettler diagram. These are shown in Fig. 8. The case shown as a red $\times$ in the lower left corner of the Guettler diagram was obtained by bowing with bow force $f_N = 0.7992$ N/m and acceleration $a = 0.3437$ m/s^2 and resulted in a double slipping motion (see Fig. 8, left). Instead, both simulations returned Helmholtz motion with a very long transient. In the case of bowing with bow force $f_N = 2.0791$ N/m and acceleration $a = 1.0481$ m/s^2, indicated by the green $\times$ in the Guettler

https://doi.org/10.1121/10.0028228

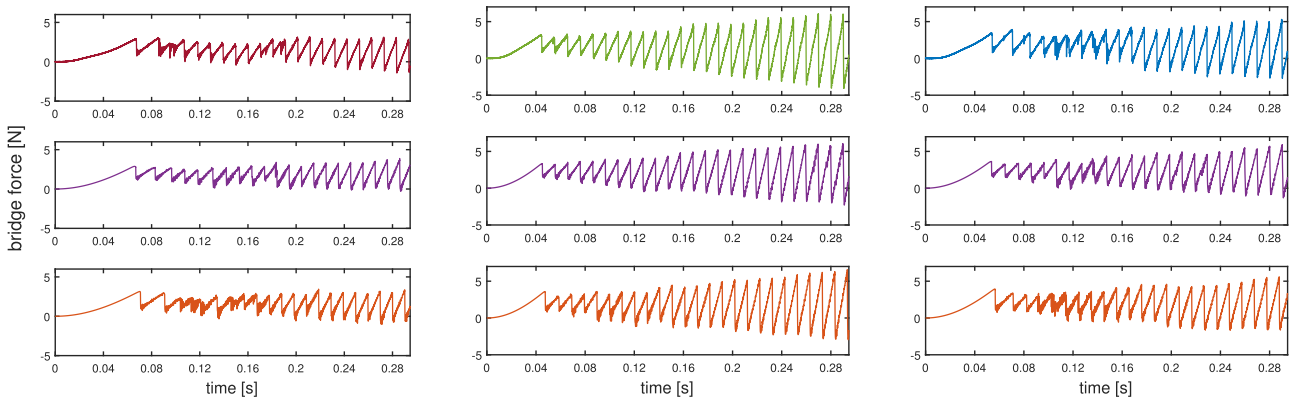

FIG. 7. (Color online) Examples of waveforms from different locations in the Guettler diagram that were well reconstructed using the derived coefficients. (Top) Measured signal. (Middle) S-model. (Bottom) ϵ- model. From left to right, the bow force and acceleration pairs are $f_N = 3.0671$ N/m and $a = 0.5576$ m/s^2, $f_N = 3.5302$ N/m and $a = 1.3821$ m/s^2, and $f_N = 3.8594$ N/m and $a = 1.0697$ m/s^2.

diagrams, both simulations predicted from the first slip a perfect Helmholtz motion, whereas the experimentally obtained waveform resulted in double slipping (see Fig. 8, middle). On the other hand, in the case of a signal obtained by bowing with a high bow force (3.9125 N/m) and high acceleration (2.0651 m/s^2), marked with a blue $\times$ in the Guettler diagrams, the models predicted two different behaviors (see Fig. 8, right): a double slip (however, of a different form from the one obtained from the measurement) using the S-model and a perfect Helmholtz motion using the ϵ-model. This reflects the fact that the simulated Guettler diagrams present a much larger playable area, in comparison to the measured one, and raises the question whether it is possible to adjust the friction model parameters in order to better resynthesize those measured signals. Such an approach is presented in Sec. V A, by allowing the friction parameters (s_0, s_1, μ_C, μ_S and v_S, or ϵ, depending on the version of the model) to vary with bow force and acceleration.

A. Friction model parameter variation

We demonstrate here how inverse modeling can enhance the reconstruction of randomly selected waveforms from the Guettler diagram. Additionally, we gain understanding into why the proposed model, along with other models found in the literature, struggle to accurately reconstruct measured Guettler diagrams.

As a first example, let us consider a waveform obtained with acceleration $a = 0.3473$ m/s^2 and bow force $f_N = 0.7992$ N/m marked with a red $\times$ on the Guettler diagram in Fig. 6. The original signal and its reconstructions using the previously optimized parameters are plotted in Fig. 8 (left). In this case, both the transient and the steady state were not reconstructed correctly with the coefficients obtained in Sec. IV. Here, the string seems to stick to the bow for too long and finally settles for Helmholtz motion instead of a double slip. An additional optimization step is included, where these parameters are used as a starting point, while the friction parameters (s_0, s_1, μ_C, andμ_S as well as v_S, respectively, ϵ) are optimized in an attempt to further minimize the objective function. Additionally, in a post-processing step, in case the optimization error remains above a certain threshold, ζ is set to 0.2. The obtained results are shown in Fig. 9 (left). It can be seen that both the steady state and the transient are now well reconstructed. The new parameters are listed in Table IV for the S-curve and in Table V for the ϵ-curve.

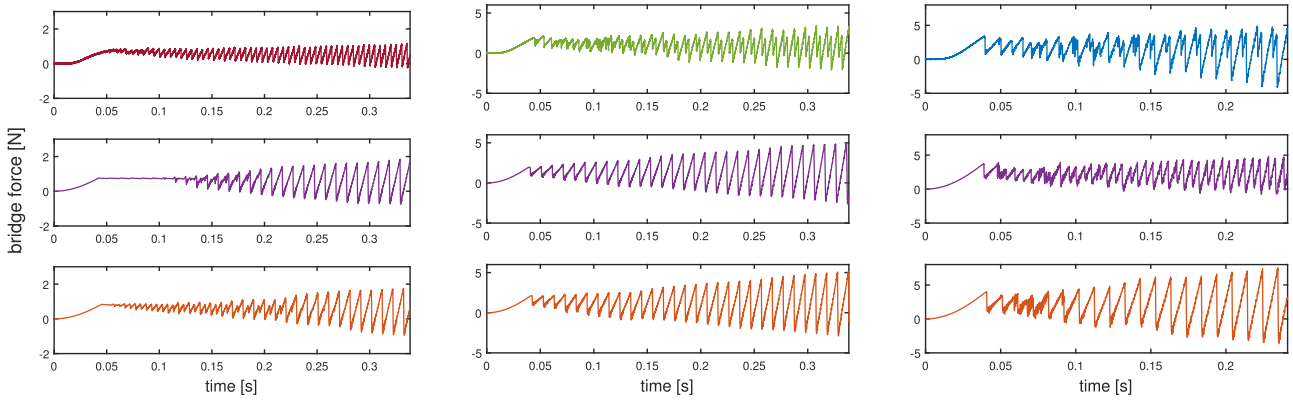

FIG. 8. (Color online) Examples of the waveforms from different locations in the Guettler diagram that were not well reconstructed using the fix coefficients. (Top) Measured signal. (Middle) S-model. (Bottom) ϵ-model. From left to right, the bow force and acceleration pairs are $f_N = 0.7992$ N/m and $a = 0.3473$ m/s^2, $f_N = 2.0791$ N/m and $a = 1.0481$ m/s^2, and $f_N = 3.9125$ N/m and $a = 2.0651$ m/s^2.

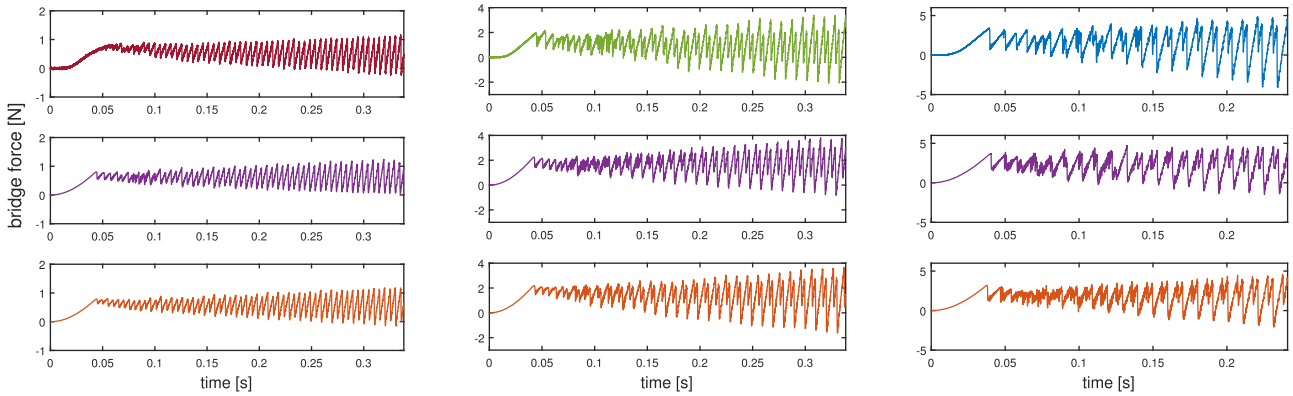

FIG. 9. (Color online) Examples of the waveforms from Fig. 8 that were reconstructed using individually optimized set of friction parameters. (Top) Measured signal. (Middle) *S*-model. (Bottom) ϵ-model. From left to right, the bow force and acceleration pairs are $f_N = 0.7992$ N/m and $a = 0.3473$ m/s^2, $f_N = 2.0791$ N/m and $a = 1.0481$ m/s^2, and $f_N = 3.9125$ N/m and $a = 2.0651$ m/s^2.

A similar procedure was employed for the two other cases marked with a green × and blue × in Fig. 6 and plotted in Fig. 8 (middle and right) together with their simulated counterparts using the previously obtained parameters. Again, in both cases, it was possible to reconstruct the measured waveform by further optimizing the friction parameters. Newly obtained signals are plotted in Fig. 9 (middle and right), while the optimized parameters are listed in Table IV for the *S*-curve and in Table V for the ϵ-curve.

In general, due to the chaotic nature of the frictional interaction, time-domain waveforms may vary within the Guettler plane for neighboring points. A way to demonstrate that is by plotting waveforms corresponding to a single column of the Guettler diagram. This is shown in Fig. 10 for measured signals (left) and simulated signals (middle and right). These contrasting waveforms at high and low bow force (for the same bow acceleration) correspond to extreme forms of the string's response, from "loose/slipping" to "choked/creaky."[32]

Based on the examples we analyzed, we can conclude that both the transient and steady state are reasonably well reconstructed using individually optimized friction parameters. We observed that the friction scheme coefficients, in particular the static and dynamic friction coefficients, should not be kept constant for varying bow force and acceleration. A cross section through the 8th column of the Guettler diagram, corresponding to an acceleration of $a = 0.8722$ m/s^2 (Fig. 11), and a cross section through the 22nd row, corresponding to a bow force of $f_N = 3.3118$ N/m (Fig. 12), show how the coefficients of friction change with varying bow force and bow acceleration. The trend that can be observed, and which is more prominent in the simulations using the *S*-model, is that the difference between static and dynamic coefficients increases with increasing bow force (see Fig. 11) and decreases with increasing acceleration (see Fig. 12). This is in some sense in agreement with observations in Ref. 2, where the author created experimental Guettler diagrams and extracted the static and dynamic friction coefficients: the static coefficient μ_S was changing with bow acceleration and the dynamic one, μ_C, with bow force. Moreover, we notice that the rate of decay of the underlying friction curve (the transition from elastic to plastic state) seems to be different for different bow force and acceleration values. A possible explanation for that behaviour could be the presence of rosin on the bow hair. Rosin is a glassy material that changes its state due to temperature changes.[1] The change in temperature depends on the relative bow-string velocity; therefore, the profile of rosin's state-changes depends on the bow acceleration (and bow force). That profile seems to be reflected in the fact that friction parameters need to vary for

TABLE IV. Table with optimized parameters for *S*-curve in the elastoplastic model.

	Result for case denoted by[a]:			
Parameter	○	Red ×	Green ×	Blue ×
a (m/s^2)	0.8722	0.3473	1.0481	2.0651
f_N (N)	2.3433	0.7992	2.0791	3.9125
s_0 (N/m)	3.186×10^5	3.706×10^5	3.332×10^5	3.0267×10^5
s_1 (kg/s)	0.0027	0.0082	0.05	0.0026
v_S (m/s)	0.228	0.0513	0.1603	0.228
μ_C	0.5071	0.7727	0.7722	0.5071
μ_S	1.0207	1.0902	1.17	1.0207

[a]○ corresponds to the black circle in the Guettler diagram. The color of × in each case corresponds to the color of the waveform shown in Fig. 9.

TABLE V. Table with optimized parameters for ϵ-curve in the elastoplastic model.

	Result for case denoted by[a]:			
Parameters	○	Red ×	Green ×	Blue ×
a (m/s)	0.8722	0.3473	1.0481	2.0651
f_N (N)	2.3433	0.7992	2.0791	3.9125
s_0 (N/m)	2.409×10^5	2.597×10^5	1.897×10^5	3.3147×10^5
s_1 (kg/s)	0.0115	0.0034	0.000 74	0.0228
ϵ	0.4	0.1	0.4	0.4
μ_C	0.3382	0.6951	0.5308	0.3365
μ_S	1.1489	1.0925	1.1725	0.9116

[a]○ corresponds to the black circle in the Guettler diagram. The color of × in each case corresponds to the color of the waveform shown in Fig. 9.

https://doi.org/10.1121/10.0028228

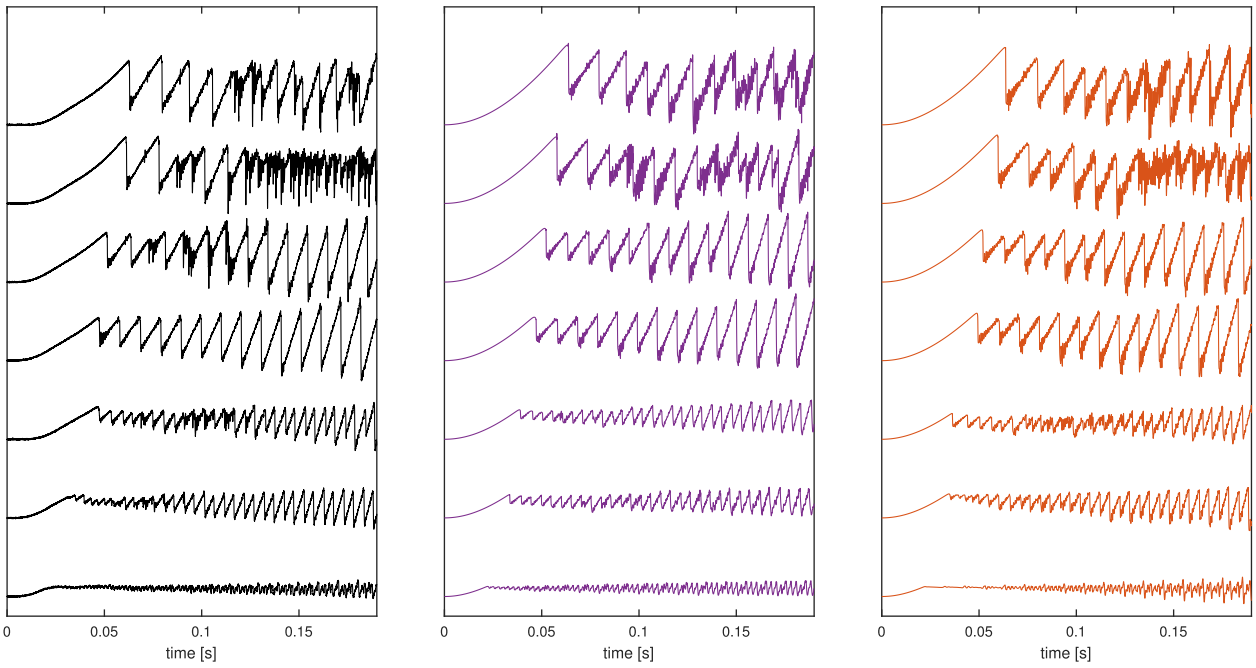

FIG. 10. (Color online) Cross section of the 8th column of the Guettlar diagram, corresponding to an acceleration of $a = 0.8722$ m/s^2. From left to right are shown the measured Guettler diagram, simulated Guettler diagram using the S-model, and simulated Guettler diagram using the ϵ-model. The bow forces are, from top to bottom, 3.8484, 3.4033, 2.9029, 2.3433, 1.6621, 1.1171, and 0.5451 N/m. The parameters for the waveforms in simulated columns were optimized for each set of bow force and acceleration.

different control conditions. This in turn suggests that in order to improve the present friction model, a state variable related to rosin could be incorporated, potentially merging the elasto-plastic model with the thermal model of Smith and Woodhouse.[1]

VI. DISCUSSION

In this work, we analysed the performance of an elasto-plastic friction model applied to bowing a string. The influence of the body of the instrument and other strings was not taken into account as the string was mounted on a monochord. The goal was to investigate if numerical reconstructions of both transients and steady state of experimentally obtained waveforms were possible and then, more globally, to investigate the performance of the model in the context of playability. Two versions of the elasto-plastic model were investigated, the models differing by the choice of the steady-state bristle displacement function z_{ss}. By employing

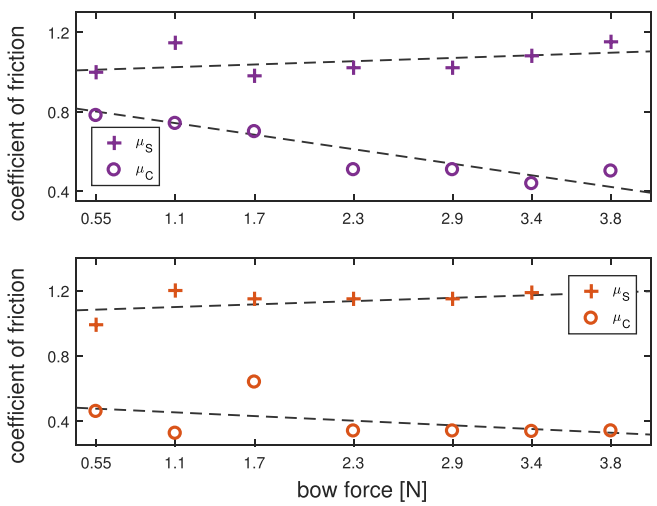

FIG. 11. (Color online) Evolution of static and dynamic friction coefficients along the 8th row of the Guettler diagram, corresponding to an acceleration of 0.8722 m/s^2. The coefficients were obtained using inverse modeling to match the corresponding measured waveforms using the S-model (top) and the ϵ-model (bottom). The dashed lines indicate a linear trend in the parameter variation.

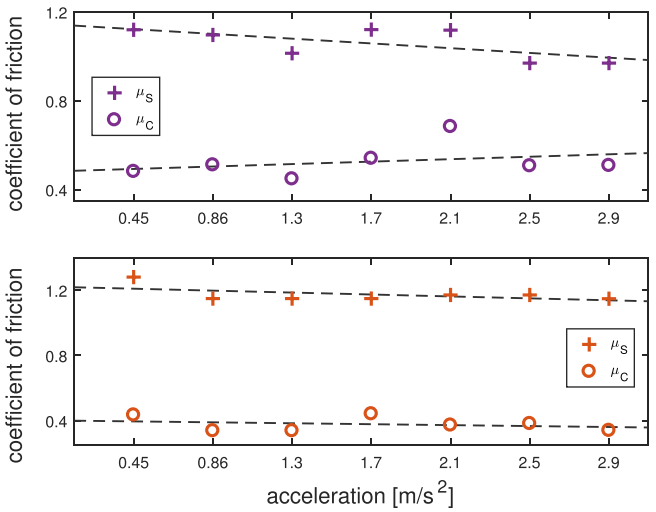

FIG. 12. (Color online) Evolution of static and dynamic friction coefficients along the 22nd row of the Guettler diagram, corresponding to a bow force of $f_N = 0.3118$ N/m. The coefficients were obtained using inverse modeling to match the corresponding measured waveforms using the S-model (top) and the ϵ-model (bottom). The dashed lines indicate a linear trend in the parameter variation.

inverse modeling, it was possible to relatively well reconstruct measured waveforms, with respect to both transient and steady state. In the process of generating simulated Guettler diagrams, we observed that a fixed—for all pairs of bow force and acceleration—set of friction parameters was not able to reconstruct individual waveforms even though the playability region of the simulated Guettler diagram agreed roughly with the measured one. The simulated Guettler diagrams were obtained using the parameters corresponding to the waveform denoted with a black circle in Fig. 1. This lies within the playable wedge and results in a Guettler diagram that shows a plausible playability region. We have also observed that using parameters corresponding to a point outside this region (e.g., corresponding to the red $\times$) does not result in a Guettler diagram with a playability region similar to that predicted from theory.

By adjusting the respective friction parameters, it was possible to reconstruct individual waveforms: the ones that exhibited Helmholtz motion as well as the ones outside the "playable" region. The model parameters that allowed for good reconstructions were obtained by inverse modeling and cannot be guaranteed to be unique. Therefore, it is hard to make meaningful conclusions on the exact value of the model parameters. Nevertheless, we observed that the parameters that varied the most with bow force and acceleration were those describing the steady-state friction curves z_{ss}^1 and z_{ss}^2, which allows the observation of certain trends. First, the limiting static and dynamic friction coefficients tend to be different for different force/acceleration combinations, and the "gap" between them tends to change as well. This trend was observed also previously in measurements.[2] Second, the underlying friction curve profile z_{ss}, which is regulated by v_S or ϵ, depending on the version of the model, also seems to depend on the combination of bow force and acceleration. One possible explanation could be the presence of rosin on the bow hair. Rosin is a material that changes its state from solid to liquid according to the temperature it is exposed to. The observation of Smith and Woodhouse[1] on the effect of rosin is that when the string slides under the bow, it heats up the rosin, which starts melting, and the friction force between the bow and the string decreases. How that temperature rises, and consequently how "fast" the rosin changes its state, depends on the relative bow-string velocity. Moreover, when the string is about to be picked up by the bow again, the rosin is warmer than at the beginning of the slipping phase; therefore, the friction force should be lower than when the string started slipping. In Ref. 30, the friction forces under the bow and string velocity are reconstructed using measurements of the bridge force, and plotting friction vs velocity confirms these assumptions.

Similar velocity-force plots have been obtained here for simulated waveforms, for both versions of the model (see Fig. 5). The hysteresis loops follow roughly the underlying steady-state friction curves z_{ss}^1 and z_{ss}^2, respectively, and therefore, for higher velocities the friction force will be equal to the value of the limiting dynamic friction coefficient μ_C. In the model, we do not explicitly mention the effect of rosin; however, it can be thought of as indirectly encoded in the bristle stiffness and damping coefficients as well as the underlying steady-state function z_{ss}. The model assumes a fixed value of the bristle stiffness coefficient s_0 throughout the simulation, regardless of the state of the string (sticking/slipping). The coefficient s_0 can be regarded as a reflection of the state the rosin is in: high s_0 means the rosin is glassy, and low s_0 means the rosin is more liquid. Intuitively, the stiffness coefficient then should change according to the temperature/velocity. Additionally, as confirmed by the reconstructions of individual waveforms in Sec. V A, the steady-state function z_{ss} should change, depending on the bow force and/or acceleration. Preliminary simulations showed that making s_0 velocity dependent showed promising results: the friction force is lower when the string is about to be picked up by the bow again. It would be interesting to see if it is possible to design a physics-based function for altering the bristle stiffness coefficient by integrating concepts from both the thermal and the elasto-plastic friction models. As such, future work could further explore the relationship between friction parameters and bow force, as well as bow acceleration, since it seems that the friction force in the elasto-plastic model should depend also on the changes in the properties of rosin.

ACKNOWLEDGMENTS

We would like to thank Alexander Mayer and Alessio Lampis for designing the experimental setup and obtaining the measured bridge force signal. This research was funded in whole or in part by the Austrian Science Fund (FWF) [10.55776/P34852].

AUTHOR DECLARATIONS

Conflict of Interest

The authors have no conflicts to disclose.

DATA AVAILABILITY

The data that support the findings of this study are available from the corresponding author upon reasonable request.

[1]J. Smith and J. Woodhouse, "The tribology of rosin," J. Mech. Phys. Solids **48**(8), 1633–1681 (2000).
[2]P. M. Galluzzo, "On the playability of stringed instruments," Ph.D. thesis, University of Cambridge, Cambridge, UK, 2004.
[3]S. Serafin, F. Avanzini, and D. Rocchesso, "Bowed string simulations using an elasto-plastic friction model," in *Proc. Stockholm Music Acoustics Conference 2003*, edited by R. Bresin, Stockholm, Sweden (2003).
[4]P. Dupont, V. Hayward, B. Armstrong, and F. Altpeter, "Single state elasto-plastic friction models," IEEE Trans. Autom. Control **47**(5), 787–792 (2002).
[5]J. Woodhouse, "Bowed string simulation using a thermal friction model," Acta Acust. united Ac. **89**, 355–368 (2003).
[6]P. Galluzzo, J. Woodhouse, and H. Mansour, "Assessing friction laws for simulating bowed-string motion," Acta Acust. united Ac. **103**(6), 1080–1099 (2017).
[7]euphonics.org, "Euphonics: The science of musical instruments," https://euphonics.org/ (Last viewed July 2, 2024).

https://doi.org/10.1121/10.0028228

[8]J. C. Schelleng, "The bowed string and the player," J. Acoust. Soc. Am. **53**, 26–41 (1973).
[9]K. Guettler, "On the creation of the Helmholtz motion in bowed strings," Acta Acust. united Ac. **88**(6), 970–985 (2002).
[10]H. Mansour, "The bowed string and its playability: Theory, simulation and analysis," Ph.D. dissertation McGill University, Montreal, Quebec, Canada, 2016.
[11]P. Galluzzo and J. Woodhouse, "High-performance bowing machine tests of bowed-string transients," Acta Acust. united Ac. **100**(1), 139–153 (2014).
[12]R. T. Schumacher and S. Garoff, "Bowing with a glass bow," J. Catgut Acoust. Soc. **3**, 9–17 (1996).
[13]J. Woodhouse, "Bowed string transients: Enhanced modelling of friction and finite-width bows," in *Proc. Stockholm Music Acoustics Conference 2023*, edited by S. D'Amario, S. Ternström, and A. Friberg, Stockholm, Sweden (2023).
[14]S. Willemsen, S. Bilbao, and S. Serafin, "Real-time implementation of an elasto-plastic friction model applied to stiff strings using finite-difference schemes," in *Proceedings of the 22nd International Conference on Digital Audio Effects (DAFx-19)*, Birmingham, UK (2019), pp. 40–46.
[15]A. Falaize and D. Roze, "A generic passive-guaranteed structure for elastoplatic friction models," in *Proceedings of the Second International Nonlinear Dynamics Conference (NODYCON21)* (online) (2021).
[16]A. Lampis, A. Mayer, M. Pàmies-Vilà, and V. Chatziioannou, "Examination of the static and dynamic forces at the termination of a bowed string," J. Acoust. Soc. Am. **153**, A198 (2023).
[17]A. Mayer and A. Lampis, "A versatile monochord setup: An industrial robotic arm as bowing and plucking device," IWK Tech Report, University of Music and Performing Arts Vienna (2024).
[18]P. Morse, *Vibration and Sound* (Acoustical Society of America, Melville, NY, 1936).
[19]N. Fletcher and T. Rossing, *The Physics of Musical Instruments*, 2nd ed. (Springer-Verlag, New York, 1998).
[20]S. Bilbao, *Numerical Sound Synthesis* (John Wiley & Sons, Hoboken, NJ, 2009).
[21]J. Bensa, S. Bilbao, R. Kronland-Martinet, and J. Smith III, "The simulation of piano string vibration: From physical models to finite difference schemes and digital waveguides," J. Acoust. Soc. Am. **114**(2), 1095–1107 (2003).
[22]C. Cuesta and C. Valette, "Evolution temporelle de la vibration des cordes de clavecin" ("Time-evolution of the vibration of the strings of a harpsichord"), Acoustica **66**(1), 37–45 (1988).
[23]C. Desvages, S. Bilbao, and M. Ducceschi, "Improved frequency-dependent damping for time domain modelling of linear string vibration," in *Proceedings of the 22nd International Congress of Acoustics—Buenos Aires*, Buenos Aires, Argentina (Argentinian Acousticians Association, 2016).
[24]R. Pitteroff and J. Woodhouse, "Mechanics of the contact area between a violin bow and a string. Part II: Simulating the bowed string," Acta Acust. united Ac. **84**, 744–757 (1998).
[25]E. Matusiak and V. Chatziioannou, "A comparison of friction models for bow-string interaction based on experimental measurements," in *Proc. Stockholm Music Acoustics Conference 2023*, edited by S. D'Amario, S. Ternström, and A. Friberg, Stockholm, Sweden (2023).
[26]R. Stribeck, "Kugellager für beliebige Belastungen" ("Ball bearings for any stress"), Z. Vereins Deutscher Ingenieure **45**, 73–79 (1901).
[27]S. Willemsen, "Real-time simulation of musical instruments using finite-difference time-domain methods," Ph.D. thesis, Aalborg University, Aalborg, Denmark, 2021.
[28]H. Olsson, "Control systems with friction," Ph.D. thesis, Lund Institute of Technology (LTH), Lund, Sweden, 1996.
[29]H. Rosenbrock, "An automatic method for finding the greatest or least value of a function," Comput. J. **3**, 175–184 (1960).
[30]J. Woodhouse, R. Schumacher, and S. Garoff, "Reconstruction of bowing point friction force in a bowed string," J. Acoust. Soc. Am. **108**(1), 357–368 (2000).
[31]R. Schumacher, S. Garoff, and J. Woodhouse, "Probing the physics of slip–stick friction using a bowed string," J. Adhes. **81**(7-8), 723–750 (2005).
[32]K. Guettler and A. Askenfelt, "Acceptance limits for the duration of pre-Helmholtz transients in bowed string attacks," J. Acoust. Soc. Am. **101**(5), 2903–2913 (1997).